Mon. Not. R. Astron. Soc. **000**, 1–13 (2017) Printed 16 February 2017 (MN LATEX style file v2.2)

On the nature of the candidate T-Tauri star V501 Aurigae ⋆

M. Vaňko,[1]† G. Torres[2], Ľ. Hambálek[1], T. Pribulla[1], L.A. Buchhave[3], J. Budaj[1], P. Dubovský[4], Z. Garai[1], C. Ginski[5], K. Grankin[6], R. Komžík[1], V. Krushevska[7], E. Kundra[1], C. Marka[8], M. Mugrauer[9], R. Neuhäuser[9], J. Ohlert[10,11], Š. Parimucha[12], V. Perdelwitz[13], St. Raetz[14], S.Yu. Shugarov[1,15]

[1] *Astronomical Institute, Slovak Academy of Sciences, 059 60 Tatranská Lomnica, Slovakia*
[2] *Harvard-Smithsonian Center for Astrophysics, 60 Garden St., Cambridge, MA 02138, USA*
[3] *Centre for Star and Planet Formation Natural History Museum of Denmark, University of Copenhagen, DK-1350 Copenhagen, Denmark*
[4] *Vihorlat Observatory, Mierova 4, Humenné, Slovakia*
[5] *Leiden Observatory, Leiden University, P.O. Box 9513, 2300 RA Leiden, The Netherlands*
[6] *Crimean Astrophysical Observatory, Scientific Research Institute, 298409, Nauchny, Crimea*
[7] *Main Astronomical Observatory, National Academy of Sciences of Ukraine, 27, Akademika Zabolotnoho, Kyiv, 03680, Ukraine*
[8] *Instituto de Radioastronomía Milimétrica, Av. Divina Pastora 7, Núcleo Central, E-18012 Granada, Spain*
[9] *Astrophysikalisches Institut und Universitäts-Sternwarte, Schillergäßchen 2-3, 07745 Jena, Germany*
[10] *University of Applied Sciences, Wilhelm-Leuschner-Strasse 13, 61169 Friedberg, Germany*
[11] *Michael Adrian Observatory, Astronomie Stiftung Trebur, Fichtenstrasse 7, 65468 Trebur, Germany*
[12] *Institute of Physics, Faculty of Science, University of P.J. Šafárik in Košice, Park Angelinum 9, 04001 Košice, Slovakia*
[13] *Hamburger Sternwarte, Gojenbergsweg 112, 21029 Hamburg, Germany*
[14] *Freiburg Institute of Advanced Studies (FRIAS), University of Freiburg, Albertstraße 19, D-79104 Freiburg, Germany*
[15] *Sternberg Astronomical Institute, Moscow State University, Universitetskij pr., 13, Moscow, 119991, Russia*

arXiv:1702.04512v1 [astro-ph.SR] 15 Feb 2017

Accepted XXXX December 15. Received 2016 August 23; in original form 2016 August 23

ABSTRACT

We report new multi-colour photometry and high-resolution spectroscopic observations of the long-period variable V501 Aur, previously considered to be a weak-lined T-Tauri star belonging to the Taurus-Auriga star-forming region. The spectroscopic observations reveal that V501 Aur is a single-lined spectroscopic binary system with a 68.8-day orbital period, a slightly eccentric orbit ($e \sim 0.03$), and a systemic velocity discrepant from the mean of Taurus-Auriga. The photometry shows quasi-periodic variations on a different, ∼55-day timescale that we attribute to rotational modulation by spots. No eclipses are seen. The visible object is a rapidly rotating ($v \sin i \approx 25$ km s^{-1}) early K star, which along with the rotation period implies it must be large ($R > 26.3$ R$_\odot$), as suggested also by spectroscopic estimates indicating a low surface gravity. The parallax from the *Gaia* mission and other independent estimates imply a distance much greater than the Taurus-Auriga region, consistent with the giant interpretation. Taken together, this evidence together with a re-evaluation of the Li I λ6707 and Hα lines shows that V501 Aur is not a T-Tauri star, but is instead a field binary with a giant primary far behind the Taurus-Auriga star-forming region. The large mass function from the spectroscopic orbit and a comparison with stellar evolution models suggest the secondary may be an early-type main-sequence star.

Key words: stars: individual: V501 Aur.

1 INTRODUCTION

V501 Aurigae (W72, 1RXS J045705.7+314234, HD 282600, TYC 2388-857-1, $V = 10.57$, $B - V = 1.62$) was detected as an X-ray source by ROSAT (Wichmann et al. 1996), and was classified by these authors as a possible new weak-lined T-Tauri star (hereafter WTTS) based on the presence of the Li I λ6707 resonance line in low-resolution optical spectra,

⋆ Based on observations obtained with telescopes of the University Observatory Jena, operated by the Astrophysical Institute of the Friedrich-Schiller-University Jena, at Michael Adrian Observatory, Germany and at Stará Lesná and Kolonica Observatory, Slovakia. Based on the data from SuperWASP and NSVS archives.

† vanko@ta3.sk

the Hα line slightly in emission, and the late spectral type (K2). Frink et al. (1997) examined the proper motion of the star and concluded that it is a likely member of the central region of the Taurus-Auriga star-forming region (SFR). Additional Li observations based on higher-resolution spectra of 35 of the candidate WTTS by Wichmann et al. (1996) were published by Martín & Magazzú (1999), who reported for V501 Aur only an upper limit to the Li equivalent width (EQW) of 90 mÅ, along with an Hα EQW of 0.9 Å *in absorption*, and the same spectral classification as the previous authors.

Wichmann et al. (2000) revisited many of the candidate WTTS from their earlier paper including V501 Aur, drawing on new high-resolution spectroscopic observations from the Harvard-Smithsonian Center for Astrophysics (CfA) as well as the ELODIE spectrograph at the Haute-Provence Observatory. They reported a new Li measurement of $\mathrm{EQW_{Li\,I}} =$ 138 mÅ from their ELODIE observations, and obtained effective temperature estimates of $T_{\rm eff} = 5350$ K and $T_{\rm eff} =$ 4897 K from a cross-correlation analysis of the CfA spectra and directly from the K2 spectral type, respectively. They reported also estimates of the rotational velocity as $v \sin i =$ 25 $\mathrm{km\,s^{-1}}$ (CfA) and $v \sin i = 27$ $\mathrm{km\,s^{-1}}$ (ELODIE). Their Li measurement was more typical of Pleiades-age stars than younger WTTS, which, together with the discovery that V501 Aur is a single-lined spectroscopic binary as revealed by the CfA spectra, led them to be more cautious in claiming WTTS status for the object. Nevertheless, on the tentative assumption that it is a member of Taurus-Auriga and is therefore at a distance of ∼140 pc, they used evolutionary models by D'Antona & Mazzitelli (1994) to estimate the luminosity ($L = 7.8$ $\mathrm{L_\odot}$), radius ($R = 3.86$ $\mathrm{R_\odot}$), and mass ($M = 1.36$ $\mathrm{M_\odot}$) of the star, and assigned it a very young age of log(age) = 5.53 ($\sim 3 \times 10^5$ yr). Additional Hα and projected rotational velocity measurements were reported by Nguyen et al. (2009) as $\mathrm{EQW_{H\alpha}} = 1.0 \pm 0.5$ Å (absorption) and $v \sin i = 25.5 \pm 1.5$ $\mathrm{km\,s^{-1}}$, in good agreement with those of Martín & Magazzú (1999) and Wichmann et al. (2000) mentioned above.

Photometric monitoring of V501 Aur has been carried out by several authors. Bouvier et al. (1997) observed it as part of a sample of 58 WTTS detected in the ROSAT All-Sky Survey (RASS). They were able to derive rotation periods for 18 of their stars, all but one being ascribed to rotational modulation by stellar spots. The one exception was V501 Aur, which showed evidence of variability on a very long timescale ($P > 37.6$ days) uncharacteristic of WTTS, and displayed no appreciable modulation in the $B-V$ colour in their observations, as would be expected in the spot scenario. They also claimed the star to be a double-lined spectroscopic binary, though this was based on a high-resolution but very low signal-to-noise ratio (SNR) spectrum taken at the Haute-Provence Observatory. Grankin et al. (2008) presented a homogeneous set of photometric measurements for WTTS extending up to 20 years. Their data were collected within the framework of the ROTOR program (Research Of Traces Of Rotation), aimed at the study of the photometric variability of pre-main-sequence (PMS) objects. The data set contains rotation periods for 35 out of 48 stars, including V501 Aur. Our target was observed in several seasons from 1994 to 2004 (see Section 2). The photometry showed wave-like variability of the object with an average period of about 55 days.

V501 Aur has also been included in an 8.4 GHz VLA survey of lithium-rich late-type stars from the RASS by Carkner et al. (1997). The object was detected as a radio source with a radio emission strength of $S_{8.4} = 0.17 \pm 0.05$ mJy. Daemgen et al. (2015) recently used the NIRI instrument on the 8m Gemini North telescope to carry out a near-infrared high angular resolution survey for stellar and sub-stellar companions in the Taurus-Auriga SFR, but reported no detections around V501 Aur. Finally, in a brief study by a subset of the present authors, Vaňko et al. (2015) presented new VRI measurements confirming the ∼55 day photometric periodicity. The photometric data obtained at University Observatory Jena and Stará Lesná Observatory between 2007 and 2013 were used. Based on the CfA spectroscopy (1996-1997) the authors found that V501 Aur is a single-lined spectroscopic binary with a nearly circular orbit, a large mass function implying a fairly massive companion, and an orbital period of 68.8 days that is distinctly longer than the photometric period. They speculated that the unseen companion may be a binary, or alternatively that the primary star may be a giant (implying a much greater distance than previously assumed), which might also explain the lack of detection of a main-sequence secondary.

Here we present additional spectroscopic and photometric observations of V501 Aur that motivate us to revisit the object with the following goals: (i) to improve the determination of its orbital elements as well as its physical parameters, including the atmospheric properties (temperature, surface gravity, and the strength of the Li and Hα lines); (ii) to better characterize the photometric variability, which is unusual for a WTTS, through a comprehensive study of all available observations; (iii) to investigate the difference between the photometric and orbital periods and its implications; and (iv) to present a coherent picture of the true nature of the system based on all available information, including a recent estimate of the parallax of V501 Aur from *Gaia* that appears to conflict with the notion of membership in the Taurus-Auriga star-forming region.

The paper is organized as follows. In Section 2 we present our new photometric observations followed by a detailed period analysis. Section 3 describes our new spectroscopic observations and reports an updated spectroscopic orbital solution. Section 4 contains a discussion of interstellar reddening. In Section 5 we review the physical properties of V501 Aur and re-examine the evidence for membership in the Taurus-Auriga SFR, presenting a coherent picture of its evolutionary state based on stellar evolution models. We conclude in Section 6 with our final thoughts.

2 PHOTOMETRIC OBSERVATIONS

The differential photometry used in this paper was carried out between 2007 and 2016 at four different observatories, two in Slovakia and two in Germany. The two in Slovakia are the Stará Lesná Observatory (G1; 49°09′10″N, 20°17′28″E) and the Kolonica Observatory (KO; 48°56′06″N, 22°16′26″E). The two observatories in Germany are the University Observatory Jena (GSH; 50°55′44″N, 11°29′03″E) and the Michael Adrian Obser-

Table 1. Overview of telescopes and instruments/detectors used to obtain the photometry of V501 Aur. D/f gives the diameter and focal length of the telescope. FoV is the field of view of the instrument. Observatory abbreviations: G1 – pavilion of the Stará Lesná Observatory, GSH – University Observatory Jena (see Mugrauer 2009; Mugrauer & Berthold 2010), MAO – Michael Adrian Observatory in Trebur, KO – Kolonica Observatory (ZIGA telescope; see Parimucha & Vaňko 2015).

Obs.	Telescope D/f [mm]	Detector CCD size	FoV [arcmin]
G1	Newton 508/2500	SBIG ST10-MXE 2184×1472, 6.8 μm	20.4×13.8
	Cassegrain 600/7500	FLI ML 3041 2048×2048, 15 μm	14×14
	Maksutov 180/1800	SBIG ST10 MXE 2184×1472, 6.8 μm	28.5×18.9
KO	Cassegrain 508/3454	MI G4-16000 4096×4096, 9 μm	36×36
MAO	Cassegrain 1200/9600	SBIG STL-6303E 3072×2048, 9 μm	10×7
GSH	Cassegrain 250/2250	SITe TK1024 1024×1024, 24 μm	37.7×37.7
	Schmidt 600/1350	E2V CCD42-10 2048×2048, 13.5 μm	52.8×52.8

vatory (MAO; 49°55′31″N, 08°24′41″E). All of the observations used Johnson-Cousins ($UBVR_CI_C$) and Bessel ($UBVRI$) filter sets. More detailed information on the individual observatories and instruments is given in Table 1.

The CCD frames were subjected to standard photometric corrections (overscan, dark, and flatfield), and we then performed aperture photometry using tasks within `IRAF`[1] (for G1 and GSH), the `C-munipack` package[2] (KO), and `Mira_Pro_7`[3] (MAO). The comparison star for all observations was HD 282599.

Additional photometric data used for this study were taken from the SuperWASP[4] and NSVS archives[5]. The WASP instruments have been described by Pollacco et al. (2006), and the reduction techniques discussed by Smalley et al. (2011) and Holdsworth et al. (2014). The aperture-extracted photometry from each camera on each night was corrected for atmospheric extinction, instrumental colour response, and system zero-point relative to a network of local secondary standards. The resulting pseudo-V magnitudes are comparable to *Tycho-2* (Høg et al. 2000) V magnitudes (Butters et al. 2010). The WASP observations for V501 Aur are from the first data release (DR1) of the WASP archive, which contains light curves from 2004 to 2008.

NSVS data for V501 Aur are available for the years 1999–2000 (object IDs 6830118 and 6841841). The NSVS magnitudes were converted to the Johnson V system using

$$m_V = \frac{1.875 \times m_{\rm NSVS} + m_B}{2.875} \ , \qquad (1)$$

where $m_B = 12.16$ is the Johnson B magnitude of V501 Aur (Høg et al. 2000). Numerical constants were adopted from Woźniak et al. (2004).

Prior to the analysis the light curves from individual observatories/instruments were corrected for small magnitude offsets, with the light curve from WASP being taken as the reference. The photometric precision of data points from all sources was in the range of 0.001–0.021 mag in the V passband. The worst precision was achieved in the SuperWASP data.

2.1 Period analysis

We have defined an observational season by the observability of our target star beginning in August and ending in April of the following year (see Table 2). The data from the first three seasons are mainly from the SuperWASP archive, and the data coverage is much greater than in later seasons. Season "0" contains only NSVS data.

For the period analysis we used the `VStar`[6] package developed by the American Association of Variable Star Observers (AAVSO). The period analysis was performed using a Date Compensated Discrete Fourier Transform (DC DFT) algorithm (Ferraz-Mello 1981). This method compensates for gaps within the data set using weighting, discriminating aliases, and allowing for frequency harmonic filtering. At first, we have applied DC DFT analysis on all SuperWASP data (because they have the best sampling and coverage) to explore wide range (0.00007 to 100 days) of possible periods in the dataset. The lowest frequency roughly corresponds to $1/(4w)$, where w was the span/window of the data. The highest frequency was set to the median interval between consecutive datapoints. The step in frequency was set equal to the lowest frequency.

No significant periods were found outside 40 – 70 days range for all observing seasons. Figure 1 presents folded light curves at the periods found for each season.

Season 3 (2007–2008) produced interesting results. The data from this season are merged SuperWASP, GSH, and G1 photometry, and the coverage is better in the SuperWASP data (see Figure 2). It is important to note that only $\sim$ 2% of data points are overlapping in this sample. The period analysis of the entire season resulted in a period of $P_3 = 54.92$ days. However, our new data from 2008 (no SuperWASP) were fitted poorly by this period. No other significant period was found in the full data set (our data + SuperWASP) of Season 3. As a test, we discarded all SuperWASP data from this season and ran an independent period analysis on the remaining data (our own), which yielded a period $P_3' = 58.21$ days. Because the number of SuperWASP data points is ∼40 times larger than the number of our own observations, we have chosen to retain only period P_3 for further study. We note, however, that the presence of P_3' is difficult to understand simply by undersampling of the data.

[1] IRAF is distributed by the National Optical Astronomy Observatories, which are operated by the Association of Universities for Research in Astronomy, Inc., under cooperative agreement with the National Science Foundation.
[2] http://c-munipack.sourceforge.net/
[3] http://www.mirametrics.com/mira_pro.htm
[4] http://wasp.cerit-sc.cz/form
[5] http://skydot.lanl.gov/nsvs/nsvs.php
[6] https://www.aavso.org/vstar-overview

Table 2. Observational seasons of V501 Aur with corresponding periods and amplitudes of the wave-like variability (sine model) in the V passband. Periods marked with an asterisk "*" were obtained from the wavelet analysis.

Season	Start	End	Duration [d]	Nights	Points	Period [d]	Amplitude [mag]	Source
0	1999-08-24	2000-03-26	214.8	52	112	58.07(3)	0.019	NSVS
1	2004-08-02	2004-09-30	59.0	43	912	59.22(4)	0.013	SuperWASP
2	2006-09-11	2007-02-15	157.7	63	2393	55.90(3)	0.046	SuperWASP
3	2007-09-29	2008-04-23	207.7	63	3165	54.92(3)	0.019	SuperWASP/GSH/G1
4	2008-10-03	2009-04-06	185.7	12	100	55.72(3)*	-	GSH
5	2010-09-23	2011-04-16	204.8	31	602	56.34(3)	0.040	G1
6	2011-08-26	2012-01-03	130.6	6	84	53.96(3)*	-	G1
7	2015-11-23	2016-03-31	128.9	15	719	59.60(4)	0.065	G1/KO/MAO
Σ	1999-08-24	2016-03-31	6063.9	285	8087	55.45(3)	0.026	

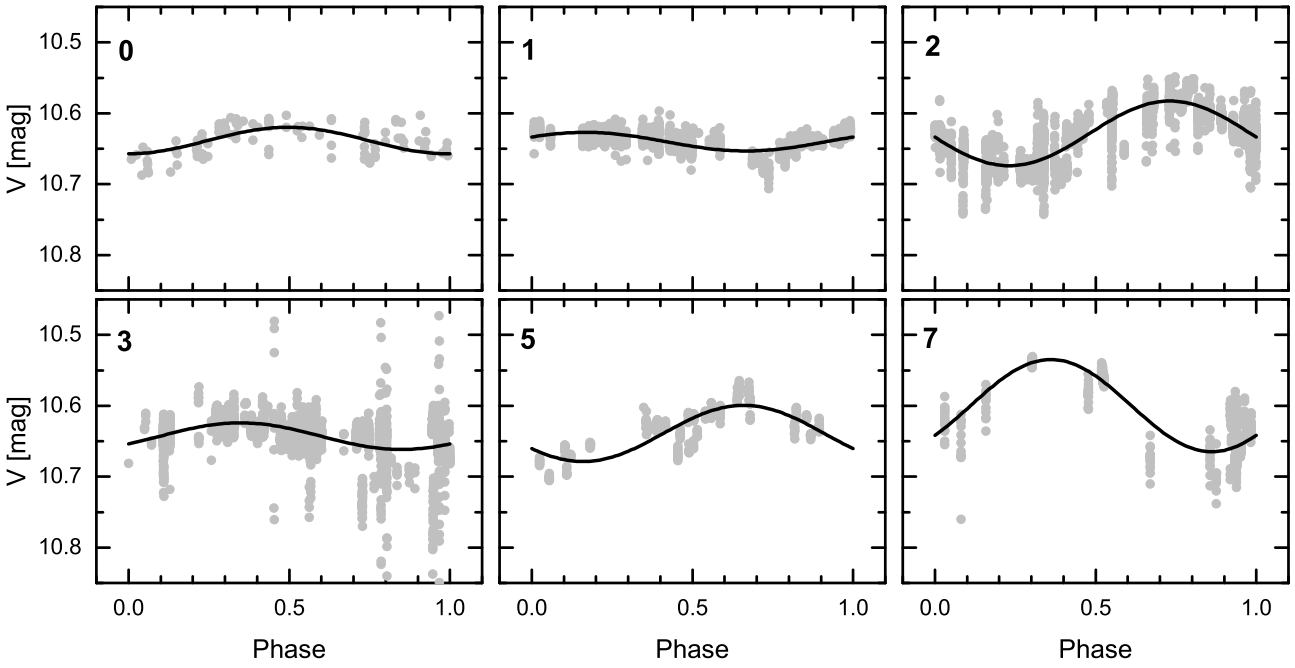

Figure 1. Results of our period analysis in individual observing seasons (indicated by the panel number). No significant period was found in Seasons 4 and 6. Each phase-folded light curve comprises of two to four cycles. The data points are distributed rather uniformly in phase in each cycle.

The original table of results by Grankin et al. (2008) showed that between 1994–1995 and 1996–1997 the observed period of the photometric wave of V501 Aur changed significantly. If a similar change occurred during our Season 3, this could perhaps explain the presence of a second periodicity. For Seasons 4 and 6 we were unable to find a significant periodicity because of considerable undersampling (see Table 2) and large gaps in the data. Below in Figure 3 we compare the periods determined in this work to those obtained by Grankin et al. (2008).

2.2 Wavelet analysis

To investigate the period variability further we have employed a standard time-frequency analysis with the Weighted Wavelet Z-Transform algorithm of Foster (1996). This algorithm is also implemented in the `VStar` package. We merged all seasons into a single data set and ran the search with a range of periods of 40–100 days, a period step of 0.1 day, and the so-called decay parameter (wavelet window) fixed at 0.001 to get better resolution for period variations. We tested several time steps ΔT = 200, 100, 50, 20, and 5 days. Because the gaps in our data set are significantly larger than the span of the seasons, we considered it important to determine how the different binning affects the shape of the wavelet. We selected from the two-dimensional wavelet the maximum values of the amplitude in selected Julian date bins, and the results are displayed in Figure 4. The analysis with a time step of $\Delta T = 5$ days diverged between Seasons 6 and 7, but all other time steps produced results that were similar. During date intervals with available data (grey areas in Figure 4) all runs produced the same results. We also tested a broader period interval, but the wavelet diverged to one of the border periods when encountering a large gap in

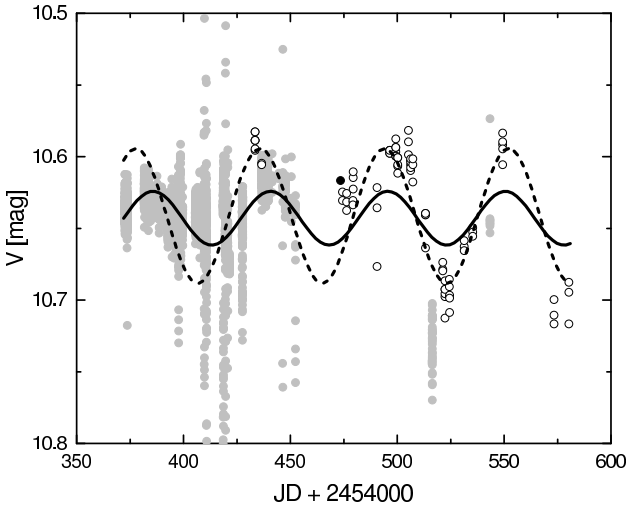

Figure 2. Fit for the period $P_3 \sim 54.92$ days (solid line) based on all data from the observational Season 3 and fit for the period $P \sim 58.2$ days found from data of this work only. The observations by SuperWASP, GSH and G1 data are shown as grey, empty and black points, respectively.

the data set. When referring to the outcome of the wavelet analysis we use results from the run with date separation $\Delta T = 20$ days.

We kept the maximum wavelet Z-values only for Julian date bins corresponding to actual data. The periods tabulated in Table 2 are in a good agreement with the wavelet analysis. Since we were unable to find periods from the period analysis for Seasons 4 and 6, we provide a rough estimate as $\sum_{i=1}^{N} Z_{\max} / \sum_{i=1}^{N} i$ where i runs through all N bins in a given season. The wavelet in Season 4 changed its value abruptly from ∼55 days to ∼85 days toward the end of the data set. We have no explanation for this. This could be caused by an intrinsic change of variability similar to that in Season 3 as discussed in the previous section. The results of the wavelet analysis and Fourier analysis (Section 2.1) are summarized in Figure 3. Finally, a folded light curve using all the data and the average period of $P = 55.45$ days (Table 2) is shown in Figure 5.

3 SPECTROSCOPIC OBSERVATIONS

Spectroscopic observations of V501 Aur were carried out with three different instruments. We began at the CfA in October 1996 using the (now decommissioned) Digital Speedometer (DS; Latham 1992) mounted on the 1.5m Tillinghast reflector at the Fred L. Whipple Observatory on Mount Hopkins (Arizona). Twenty-four spectra were recorded from September to November 1997. Some of these were used in the studies of Wichmann et al. (2000) and Vaňko et al. (2015) cited in Section 1. The resolving power of this instrument was $R \sim 35\,000$, containing a single échelle order 45 Å wide centered on the Mg I triplet (5165.8–5211.2 Å). Reductions were carried out with a dedicated pipeline, with the wavelength solution being set by exposures of a Thorium-Argon lamp before and after each science exposure. The velocity zero-point of this instrument was monitored with exposures of the dusk and dawn sky, and small run-to-run corrections were applied to the velocities described below as explained by Latham (1992). The SNRs of these observations range from 10 to 30 per resolution element of 8.5 km s^{-1}. All spectra appear single-lined.

Nine additional spectra were gathered from October 2014 to February 2015 with the Tillinghast Reflector Échelle Spectrograph (TRES; Fűrész 2008) on the same telescope. This bench-mounted, fiber-fed instrument provides a resolving power of $R \sim 44\,000$ in 51 orders over the wavelength range 3900–9100 Å. SNRs at 5200 Å ranged from 21 to 44 per resolution element of 6.8 km s^{-1}. Reductions and wavelength calibrations followed a procedure similar to that described above. IAU radial velocity (RV) standards were observed each night to monitor the velocity zero point.

Between September 2014 and April 2016 we obtained a further 25 spectra with the 60-cm Cassegrain telescope at the Stará Lesná Observatory (G1 pavilion) using the fiber-fed échelle spectrograph eShel (Pribulla et al. 2015). The spectra consisting of 24 orders cover the wavelength range from 4150 to 7600 Å. The resolving power of the spectrograph is $R = 10\,000$–$12\,000$. The reduction of the raw frames and extraction of the 1D spectra have been described by Pribulla et al. (2015). The wavelength reference system, as defined by the preceding and following Thorium-Argon exposures, was stable to within 0.1 km s^{-1}. The SNRs of the spectra at 5500 Å range from 11 to 42 (see Table 3).

3.1 Radial velocities

3.1.1 CfA data

Radial velocities from the CfA/DS and CfA/TRES spectra were obtained by cross-correlation using the IRAF task `XCSAO` (Kurtz 1992). Only the order centered on the Mg I triplet was used for both sets of spectra, for consistency. An appropriate template was selected as described later from an extensive library of pre-computed synthetic spectra (see Nordström et al. 1994; Latham 2002), with the following parameters that are close to the final values adopted in this work: effective temperature $T_{\rm eff} = 4750$ K, surface gravity $\log g = 2.5$, rotational velocity 25 km s^{-1}, and solar metallicity. Radial velocities from the two instruments were placed on the same reference frame to well within 0.1 km s^{-1}. Results in the heliocentric frame are listed in Table 3.

Preliminary orbital fits to these radial velocities indicated a large mass function, suggesting a massive secondary. Consequently, we made an effort to detect this star in these spectra employing the two-dimensional cross-correlation technique TODCOR (Zucker & Mazeh 1994) and a broad range of trial templates for the secondary star. We found no convincing evidence of a second set of lines down to a flux ratio of approximately 0.05. The Mg triplet region was used for two principal reasons: (i) experience has shown that this order has the most information on the radial velocity (large number of strong metallic lines); (ii) our synthetic template spectra are optimized for, and only cover that region. They are based on a line list that was painstakingly tuned to match real stars in this wavelength region.

An additional attempt to detect the secondary component was made using the broadening function technique (Rucinski 1992). Portions of the TRES spectra in the range 4900–5500 Å were first deconvolved using several K-type

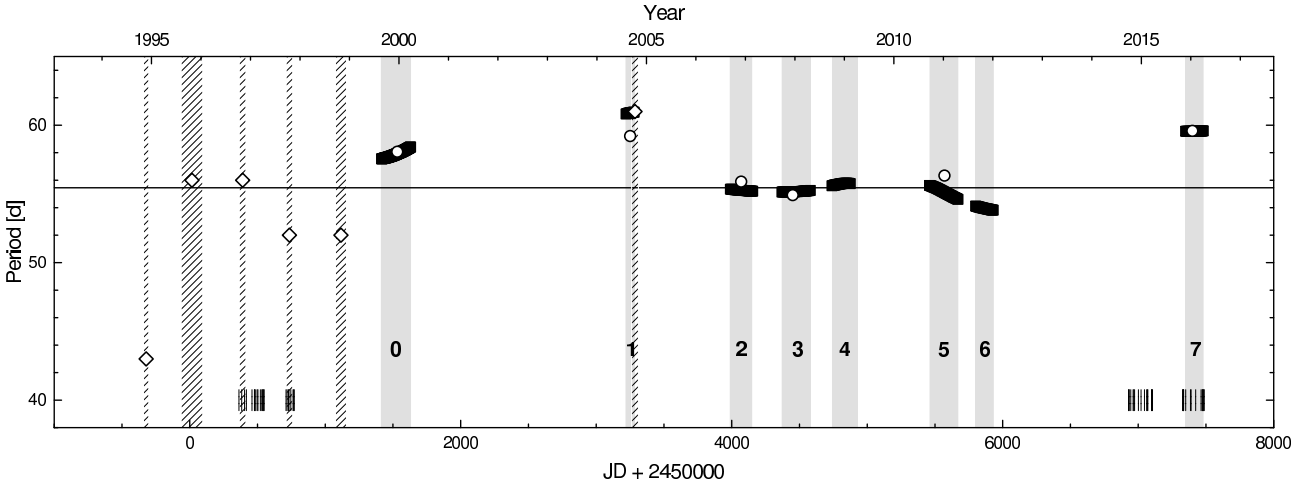

Figure 3. Long-term variability of V501 Aur. The span of observations within each season is denoted by hatched pattern (data from Grankin et al. 2008) and light grey areas (this work). Period estimates derived per single season are plotted with diamonds (data from Grankin et al. 2008) and circles (this work). The horizontal line represents the average period resulting from the entire data set (55.45 days). Maximum values of the Z-transform of the wavelet analysis are shown with black squares. Short vertical lines along the bottom denote times of spectroscopic observations. See Section 2.2 for details.

Table 3. Heliocentric radial velocities of V501 Aur from CfA and G1. Also listed are the estimated uncertainties and the SNRs at 5200 Å (DS and TRES) or 5500 Å (eShel).

HJD 2 400 000+	RV [km s^{-1}]	σ [km s^{-1}]	SNR	source	HJD 2 400 000+	RV [km s^{-1}]	σ [km s^{-1}]	SNR	source
50362.9153	−13.8	1.0	11	DS	56966.7880	−23.3	0.8	24	TRES
50383.8742	12.8	0.8	12	DS	56972.8815	−8.5	0.4	33	TRES
50404.7680	−28.6	0.9	12	DS	57001.7760	−2.6	0.4	41	TRES
50417.7154	−41.4	0.9	11	DS	57020.8238	−40.1	0.5	21	TRES
50459.5785	2.3	1.1	10	DS	57045.7911	0.9	0.4	38	TRES
50477.7025	−36.6	0.8	13	DS	57062.8015	11.0	0.5	22	TRES
50478.5889	−36.7	0.9	15	DS	57068.2735	1.9	0.6	22	eShel
50486.6598	−39.6	1.2	13	DS	57071.3213	−4.5	0.4	34	eShel
50497.6765	−18.8	0.8	11	DS	57098.3689	−35.4	0.6	21	eShel
50503.5285	−5.6	1.1	11	DS	57099.2818	−33.7	0.7	19	eShel
50521.5218	12.7	1.5	12	DS	57102.2896	−27.3	0.5	28	eShel
50532.5676	−4.5	1.2	11	DS	57105.2564	−20.6	0.6	22	eShel
50536.6212	−15.2	0.9	11	DS	57327.5888	11.2	0.3	38	eShel
50541.5795	−25.9	1.1	10	DS	57330.5687	12.9	0.7	19	eShel
50543.5327	−31.2	0.8	11	DS	57331.6593	13.1	0.3	42	eShel
50549.5373	−39.8	1.1	11	DS	57332.6283	12.7	0.5	26	eShel
50710.8428	−3.4	0.6	18	DS	57335.6321	11.9	1.2	11	eShel
50718.8748	10.2	0.8	17	DS	57350.4565	−13.1	0.5	24	eShel
50728.7420	13.3	0.8	14	DS	57350.5393	−13.6	0.4	31	eShel
50732.8548	7.6	0.7	16	DS	57385.3840	−8.9	0.9	15	eShel
50745.7864	−20.8	0.7	16	DS	57390.4150	2.9	1.1	12	eShel
50762.9408	−37.1	0.5	30	DS	57424.3079	−25.9	0.7	20	eShel
50764.7501	−36.5	0.9	12	DS	57464.2662	8.6	0.6	21	eShel
50771.7938	−23.0	0.9	12	DS	57472.2826	11.5	0.7	20	eShel
56928.6225	4.9	0.6	22	eShel	57476.2661	9.3	0.5	29	eShel
56930.6061	2.7	0.5	27	eShel	57477.2859	8.8	0.6	23	eShel
56933.0178	−3.3	0.4	34	TRES	57479.2961	5.4	0.8	16	eShel
56944.9627	−29.9	0.5	34	TRES	57484.2870	−5.8	0.6	20	eShel
56961.9875	−33.1	0.4	44	TRES	57486.2934	−8.8	0.6	21	eShel

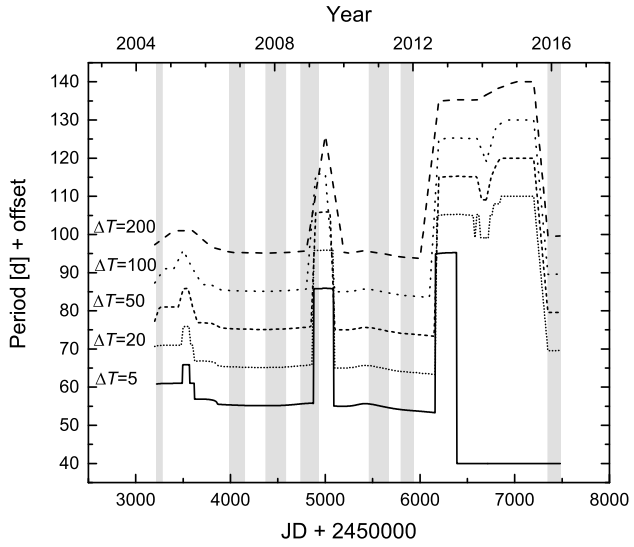

Figure 4. Comparison of different runs of our wavelet analysis. Individual runs are separated by an offset of 10 days. Grey areas show the actual seasons with available data.

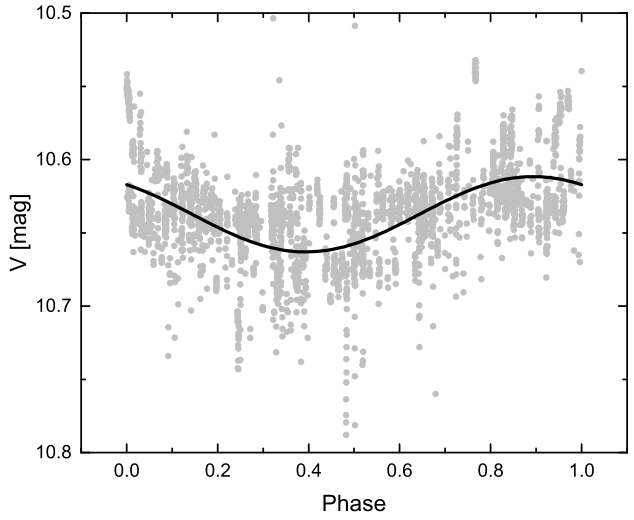

Figure 5. Phase diagram for all available data of V501 Aur folded with the average period of $P = 55.45$ days.

slowly rotating dwarfs as templates. The resulting broadening functions (BFs) always showed a single component rotating at $v \sin i = 24.7 \pm 0.7$ km s^{-1} (the primary star). Use of a K2V template (HD 3765) revealed a weak additional component with an intensity ratio $L_2/L_1 \sim 0.01$. However, the radial velocity of this component was found to be constant in the geocentric frame, and likely results from telluric lines in the red part of the spectrum. The detection limits from this exercise depend mainly on the unknown projected rotational velocity of the secondary, and faint and rapidly rotating stars are considerably more difficult to detect. If the secondary rotates with the same projected velocity as the primary, the detection limit is then estimated to be $L_2/L_1 \sim 0.05$–0.10.

The extracted BFs were inspected to see the presence of dark spots indicated by the photometric wave. The BF changes are marginal and not conclusive. For $R = 44\,000$ we can resolve only 8 pixels across the rotational profile in the velocity space. To conclusively prove the presence of the spots, more spectra of a higher resolution and SNR would have to be taken within one orbital period.

3.1.2 Stará Lesná data

Two approaches were used to derive the RVs from the G1 data: (i) cross-correlation against the spectrum of V501 Aur with the highest SNR serving as a template, and (ii) the BF technique, with BFs extracted using as a template the spectrum of HD 65583 (K0V, $v \sin i = 3.3 \pm 1.7$ km s^{-1}, [Fe/H] = -0.70). For the cross-correlation analysis we avoided spectral regions affected by strong telluric features and used only the wavelength ranges 4700–5860 Å, 5970–6260 Å, 6330–6860 Å, and 6975–7130 Å. For the BF extraction we used only the green-yellow part of the spectrum from 4900 to 5500 Å, including the Mg I triplet. Because the spectral resolution in this case is comparable to the $v \sin i$ of V501 Aur, a simple Gaussian function was fitted to both the cross-correlation functions (CCFs) and the BFs to determine the velocities.

The RVs derived from BFs were shifted to the IAU system using RV = 13.2 km s^{-1} for HD 65583 (Evans, 1979). The RVs obtained by cross-correlation were shifted to be consistent with the IAU system using the difference between the systemic velocities from preliminary orbital fits (the shift was ΔRV = 12.8 km s^{-1}). The spectroscopic elements from these fits obtained for both cases (CCFs and BFs) were consistent within 1–2σ, but the RVs derived from the BFs resulted in a slightly smaller residual standard deviation from the orbital fit (0.47 km s^{-1} for BFs vs. 0.53 km s^{-1} for CCFs), and were thus adopted for the final orbital solution.

3.1.3 Spectroscopic orbit

Prior to performing a combined solution of the CfA and G1 observations we tested the consistency of the RV reference systems by fitting spectroscopic orbits to each data set separately. Only a small difference in the systemic velocities was found (∼0.3 km s^{-1}), so the data sets were combined without adjustments. The resulting spectroscopic orbital elements for the merged data along with the predicted times of spectroscopic conjunction are listed in Table 4. A graphical representation of the measured radial velocities and orbit model is shown in Figure 6. The orbital period is very well determined because of the 7123-day (nearly 20-year) time span of the velocities (∼103 revolutions). The orbital eccentricity is small but statistically significant, and consistent between the CfA and G1 data sets.

3.2 Atmospheric parameters

The main atmospheric properties of V501 Aur, $T_{\rm eff}$, $\log g$, and metallicity, were determined in several different ways. A first method used the `iSpec` software (Blanco-Cuaresma et al. 2013) applied to two of the TRES spectra with the highest SNR, taken on October 31 and December 10, 2014, and focusing on the spectral range 4800–5300 Å. The effective temperature was determined from the line-strength ratio of Cr I 4254 Å to Fe I 4250 Å and Fe I

Table 4. Spectroscopic orbital elements of the primary component of V501 Aur based on radial-velocity measurements from CfA and G1. The uncertainty is given in parentheses in units of the final digit. $T_{\min \mathrm{I}}$ and $T_{\min \mathrm{II}}$ are the predicted times of primary and secondary eclipse (spectroscopic conjunctions). The columns present separate solutions from the CfA, G1, and combined data sets. Heliocentric Julian dates (HJD) for periastron passage are given relative to HJD 2 400 000.

Parameter	CfA	G1	Combined
P_{orb} [d]	68.8347(14)	68.824(27)	68.8333(12)
e	0.020(7)	0.047(11)	0.030(5)
ω [rad]	3.2(3)	3.16(15)	3.13(15)
T_0 [HJD]	56 955(3)	56 954.1(17)	56 953.9(16)
V_γ [km s^{-1}]	−12.53(12)	−12.85(20)	−12.71(8)
K_1 [km s^{-1}]	27.04(19)	27.1(4)	26.78(13)
$T_{\min \mathrm{I}}$ [HJD]	56 937(3)	56 937.8(17)	56 937.5(16)
$T_{\min \mathrm{II}}$ [HJD]	56 971(5)	56 970.1(25)	56 970.6(23)
$a_1 \sin i$ [au]	0.1710(12)	0.1715(26)	0.1693(8)
$f(m)$ [M$_\odot$]	0.142(3)	0.143(6)	0.1373(20)

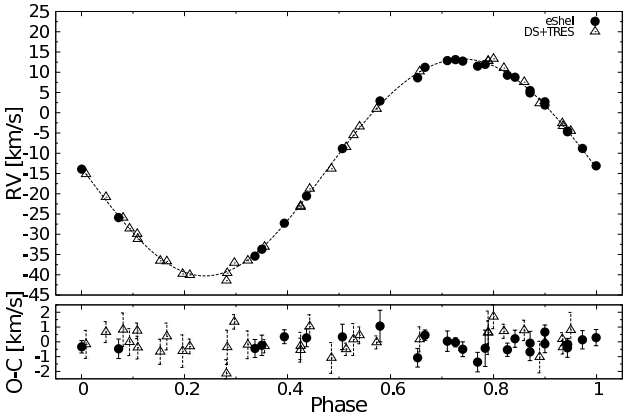

Figure 6. Spectroscopic orbit of the primary component of V501 Aur. Phase 0.0 corresponds to periastron passage. Filled symbols represent radial velocities from G1, and empty ones are from the CfA. For clarity the error bars are only shown for the residuals (bottom panel).

4260 Å (see Digital Classification Spectral Atlas[7]), using template spectra with well-established spectral types of K2V (HD 3765), K3V (HD 128165), K4V (HIP 073182), and K5V (61 Cyg A). In order to minimize the number of free parameters the projected rotational velocity was held fixed at the value $v \sin i = 24.7$ km s^{-1} determined from the BF fitting. The resulting parameters were $T_{\mathrm{eff}} = 5130 \pm 410$ K, $[\mathrm{M/H}] = 0.03 \pm 0.29$, and $\log g = 3.0 \pm 0.7$, which are somewhat uncertain. The EQW ratio of the spectral lines mentioned above showed the best match for the K2V template.

A second determination was carried out by cross-correlating each of the DS spectra against the library of synthetic spectra, to find the best match as a function of the template parameters T_{eff}, $\log g$, and $v \sin i$. Solar metallicity was assumed. The best match was determined from the peak value of the CCF averaged over all 24 spectra. Because of degeneracies caused by the narrow 45 Å window, it is generally difficult to establish the temperature and $\log g$ at the same time from these spectra: lowering the temperature and at the same time lowering the $\log g$ results in a fit of similar quality, particularly when the SNR is low. We applied the same approach to the nine TRES spectra, which have better SNR and also a wider wavelength coverage around 100 Å in the Mg I order. The resulting average parameters for V501 Aur from these determinations are $T_{\mathrm{eff}} = 4900 \pm 150$ K, $\log g = 2.7 \pm 0.6$, and $v \sin i = 27 \pm 2$ km s^{-1}. Because the temperature is also sensitive to the adopted metallicity, which is not known very well, we have chosen to assign a more conservative T_{eff} uncertainty of 250 K.

We also carried out an independent analysis of eight of our best TRES spectra using the Stellar Parameters Classification tool (SPC; Buchhave et al. 2012, 2014) obtaining the following results: $T_{\mathrm{eff}} = 4685 \pm 100$ K, $\log g = 2.27 \pm 0.24$, $[\mathrm{M/H}] = -0.42 \pm 0.11$, and $v \sin i = 28.2 \pm 2.0$ km s^{-1}. These estimates are subject to similar degeneracies as mentioned above.

The low surface gravity characteristic of giant stars was independently tested using the luminosity-sensitive line ratio between the Y II 4376 Å and Fe I 4383 Å lines, as recommended in the Digital Classification Spectral Atlas for G8 stars. A spectrum close to the lines in question was synthesized using `iSpec` for several values of the surface gravity. The comparison of the observed and synthetic spectra supports the classification of the visible component of V501 Aur as a sub-giant or a giant. However, discriminating between values of the surface gravity in the range $\log g = 1$–3 is difficult.

The EQW of the Li I λ6707 line was measured in each of our nine high-resolution TRES spectra, which show the feature clearly. The result, 90±6 mÅ, is significantly lower than the value of 138 mÅ reported by Wichmann et al. (2000), although the latter is based on spectra of low SNRs (10–15) and according to those authors may have an uncertainty of up to 40 mÅ. Unfortunately the line cannot be measured reliably in our medium-dispersion spectra with eShel because the blaze function has its minimum close to the location of this feature. Finally, we examined the Hα line in both our TRES and eShel spectra and found that it is never seen in emission over the year and a half of observation with those two instruments, contrary to what was reported originally by Wichmann et al. (1996). The average EQW from our TRES spectra is 0.97 ± 0.07 Å, similar to the measure by Martín & Magazzú (1999).

4 INTERSTELLAR EXTINCTION AND DISTANCE

The determination of the extinction towards V501 Aur is complicated by possible dust clumps in the young star-forming region against which the star is projected. It has been shown that the EQW of the Na I D1 line at 5896 Å allows for a useful estimate of the $E(B-V)$ reddening. For example, Poznanski et al. (2012) provided the empirical relation

$$\log E(B-V) = 2.47 \times \mathrm{EQW}_{\mathrm{Na\,I\,D1}} - 1.76 \pm 0.17 \qquad (2)$$

[7] https://ned.ipac.caltech.edu/level5/Gray/Gray_contents.html

with $\mathrm{EQW_{Na\,I\,D1}}$ expressed in units of Å. We used four of our nine TRES spectra in which the stellar and interstellar components of the D1 line are sufficiently separated, and fit double-Gaussians to the normalized spectra, obtaining an average $\mathrm{EQW_{Na\,I\,D1}} = 353$ mÅ. The equation above then leads to $E(B-V) = 0.13 \pm 0.06$. Alternatively, the look-up table provided by Munari & Zwitter (1997) results in a similar value of $E(B-V) = 0.15$. We note, however, that the interstellar D1 line is saturated in our spectra, implying that the above reddening estimates are only lower limits.

The *Gaia* mission (Gaia Collaboration 2016) has recently provided a measure of the trigonometric parallax of V501 Aur as $\pi = 1.258 \pm 0.397$ mas, corresponding nominally to a distance range of about 600–1160 pc. Despite the significant uncertainty, this indicates the star is not a member of the Taurus-Auriga star-forming region, as has been claimed before (see Section 1) but lies instead in the background. The new distance estimate along with the 3D dust map from Pan-STARRS (Green et al. 2015) allow for a more reliable measure of the reddening to be obtained. At the location of V501 Aur, only 7 degrees south of the Galactic plane, the result is $E(B-V) = 0.54 \pm 0.04$.

This reddening estimate is potentially useful to derive an independent measure of the effective temperature from colour indices, for comparison with the various spectroscopic determinations. Unfortunately, however, colour measurements in the optical such as the $B-V$ index differ considerably depending on the source, possibly due to variability, or are rather uncertain, and are therefore unreliable. For example, the *Tycho-2* measurements (Høg et al. 2000) yield $B-V = 1.29 \pm 0.21$ after transformation to the Johnson system, while the AAVSO Photometric All Sky Survey (APASS; Henden et al. 2014) reports $B-V = 1.71 \pm 0.13$. Intermediate values have been given by others, such as $B-V = 1.62$ (Grankin et al. 2008) and $B-V = 1.47 \pm 0.27$ (Kharchenko et al. 2009).

Near-infrared colours are less affected by reddening. For the 2MASS $J-K_s$ index, we find using our above $E(B-V)$ estimate that $E(J-K_s) = 0.523 \times E(B-V) = 0.282 \pm 0.021$ (Cardelli et al. 1989, Table 3). Applying this correction to the apparent $J-K_s$ colour of V501 Aur, $J-K_s = 0.948 \pm 0.031$, results in a de-reddened value of $(J-K_s)_0 = 0.666 \pm 0.037$ in the 2MASS system. Tabulations for giant stars by Ducati et al. (2001) and Gray (1992) then yield an effective temperature range of 4750–4950 K, consistent with our earlier spectroscopic estimates.

5 THE NATURE OF THE SYSTEM

5.1 Membership in the Taurus-Auriga SFR

As described in Section 1, V501 Aur has been claimed to belong to the central area of the Taurus-Auriga SFR (Wichmann et al. 1996; Frink et al. 1997; Wichmann et al. 2000) mainly on the basis of its detection in X-rays (ROSAT), the presence of the Li I λ6707 line in absorption, the late spectral type (K2), the reported emission in Hα, and a proper motion apparently consistent with the average value for the complex. Further properties of the star have been inferred in these studies from the assumption of a distance of 140 pc to the SFR. However, much of the evidence for a pre-main-sequence status is somewhat circumstantial.

Information gathered since, as well as observations reported here, paint a rather different picture of the nature of the system that we now describe. The principal facts supporting the new interpretation are the following, in order of relevance:

- The first public data release (DR1) from the *Gaia* mission has supplied the trigonometric parallax of V501 Aur as $\pi = 1.258 \pm 0.397$ mas, corresponding a nominal distance of $d = 795^{+366}_{-191}$ pc, or a range of approximately 600–1160 pc. This appears to rule out a membership in the Taurus-Auriga SFR ($d = 115$–156 pc, according to Grankin 2013), and places the star in the background. The formal parallax uncertainty given above excludes a component of systematic error (∼0.3 mas) that the *Gaia* Collaboration has recommended be factored into the total uncertainty (Gaia Collaboration 2016). If added quadratically to the internal error, it yields a slightly larger distance range of 570–1300 pc, still ruling out a membership in Taurus.
- An independent estimate of the distance may be derived if we interpret the photometric wave as being caused by rotational modulation due to cool photospheric spots on the visible component (see next section). In that case, the measured projected rotational velocity along with the measured photometric period yield a lower limit to the radius of the star, $R \sin i = \frac{P_{\rm rot}}{2\pi} v \sin i$, which combined with an effective temperature estimate provides a lower limit to the bolometric luminosity. This, in turn, can be used to infer a lower limit to the distance. An absolute lower limit to R is obtained by using our smallest estimate of $v \sin i = 24.7$ km s^{-1} and the shortest photometric period from Table 4, $P_{\rm rot} \approx 53.9$ days, resulting in $R \sin i \approx 26.3$ R$_\odot$. This already seems considerably larger than expected for a PMS star of any reasonable mass. Our coolest temperature estimate, $T_{\rm eff} = 4685$ K, then implies that the luminosity of the star must be at least 300 L$_\odot$. If we assume no extinction, and adopt the most recent value (and one of the brightest) of the apparent visual magnitude available for V501 Aur ($V = 10.57 \pm 0.12$; Henden et al. 2014) along with a bolometric correction of $BC_V = -0.48 \pm 0.10$ for a star of this temperature (Flower 1996; Torres 2010), we obtain an absolute lower limit to the distance of 2050 ± 180 pc. Using $V = 10.88 \pm 0.08$ (the faintest measurement in literature; Høg et al. 2000) we obtain distance of 2350 ± 200 pc. Accounting for extinction according to $A_V = 3.1\, E(B-V)$ reduces this to 950 ± 100 pc and 1100 ± 100 pc, respectively; which is consistent with the *Gaia* estimate and still much larger than the distance to Taurus-Auriga. This supports the conclusion that V501 Aur is far behind the SFR.
- Our orbital solution for V501 Aur (Table 4) yields a systemic velocity of -12.70 ± 0.08 km s^{-1} that is inconsistent with the mean radial velocity of the Taurus-Auriga SFR ($+9.8 < \mathrm{RV} < +17.5$ km s^{-1}; Mooley 2013), arguing strongly against a membership.
- The EQW of the Li I λ6707 line as measured from our nine TRES spectra, 90 ± 6 mÅ, is lower than is typical for a very young object of this temperature (see Fig. 2 of Wichmann et al. 2000), making the PMS status unlikely. We also do not find Hα to be in emission in our spectra, as is usually the case for WTTS. Compared to other evolved stars the lithium abundance of V501 Aur is high, but not exceptional (see Randich et al. 1999). Drake et al. (2002) list

a few rapidly-rotating giants showing large Li abundances and enhanced activity (indicated by X-ray luminosity and Ca II emission) similar to V501 Aur.

• Most spectroscopic estimates of the surface gravity of the visible star from our analysis ($\log g = 2.3$–3.0) are considerably lower than expected for very young objects, again pointing towards the view that V501 Aur is an evolved star rather than a PMS star.

• The measured proper motion of V501 Aur is rather small and thus not a very reliable indicator of a membership in Taurus-Auriga. Frink et al. (1997) reported $(\mu_\alpha \cos\delta, \mu_\delta) = (-2.0 \pm 4.4, -20.0 \pm 4.4)$ mas yr^{-1}, and considered this to be consistent with the mean proper motion for the SFR of $(+4.0, -18.7)$ mas yr^{-1}. More recent estimates from *Tycho-2* give a smaller total motion of $(-5.4 \pm 2.3, -11.9 \pm 2.3)$ mas yr^{-1}, and *Gaia*/DR1 lists the star as having an even smaller motion of $(-8.3 \pm 2.6, -3.4 \pm 1.9)$ mas yr^{-1}. Given that the proper motions of the true members show considerable scatter, and that there is also a significant difference between the central parts of Taurus-Auriga, $(+2.4, -21.2)$ mas yr^{-1}, and the southern region, $(+10.1, -9.8)$ mas yr^{-1}, the proper motion criterion for V501 Aur is largely inconclusive.

The above evidence strongly supports the notion that V501 Aur is a background giant, rather than a young member of the Taurus-Auriga SFR.

5.2 Photometric variability

Given the binary nature of V501 Aur, we searched for eclipses near the predicted times of spectroscopic conjunction but found none. Here we discuss other mechanisms that might explain the quasi-periodic brightness changes (see Sections 2.1 and 2.2).

Ellipsoidal variability caused by distortions in the large primary star seem rather unlikely in view of the long orbital period. The modulation would also be strictly periodic with a period exactly half that of the orbital period, $P/2 \approx 34.4$ days. A detailed search in the vicinity of this value using the more numerous superWASP data with the best temporal coverage, as well the entire photometric data set, showed no convincing evidence of a signal at this period. Numerical simulations of the expected amplitude of such an effect based on approximate stellar properties for the primary star and the companion as inferred in the next section indicate a peak-to-peak variation of only about 1% in the V band. This is at the level of the noise in the observations, which may explain the non-detection. It is also much smaller than the brightness changes actually observed in V501 Aur, so it cannot be the principal cause of those variations.

Pulsation, either in the primary or less likely in the unseen secondary, is another possibility. Our period analysis shows no coherent signals in the power spectrum. The long timescale of the variations (∼55 days) and the small colour changes ($\Delta(V-I) \approx 0.05$ mag) are consistent with the characteristics of some semi-regular variables (specifically with those of the SRd type; see the GCVS, Kholopov et al. 1985), although the amplitude of the variations in V501 Aur (0.013–0.082 mag) is smaller than is typical for such objects, and the rapid rotation is also unusual for this class.

The overall features of the photometric variability seem most consistent with modulation from photospheric spots on the visible component, perhaps appearing at different latitudes in a star with differential rotation. The observations show that the amplitude of the variations decreases toward the red, which is consistent with the spot scenario. That the star is active seems supported by the strong X-ray emission (ROSAT). Further evidence for spots could be obtained in principle through further analysis of the BFs, or trailing spectra with higher SNR and high spectral resolution. More quantitative modeling of the spots may require multi-colour photometry and considerably better time sampling than we presently have.

5.3 Physical parameters

The lack of eclipses in V501 Aur prevents a direct determination of the fundamental properties of the components, such as the masses and radii, from our spectroscopic and photometric observations. As a result, the nature of the secondary component is unclear. The large velocity semi-amplitude of the primary ($K_1 = 26.8$ km s^{-1}) results in a fairly large mass function $f(m) = 0.1373 \pm 0.0002$ M$_\odot$ and a correspondingly large minimum mass for the secondary, $M_2 \sin i = 0.516(M_1 + M_2)^{2/3}$ M$_\odot$. It is somewhat surprising, therefore, that we see no trace of the secondary lines in our spectra despite our attempts at detection (Section 3.1.1). One possibility is that the secondary is itself a close binary system. On the other hand, if the primary is a giant star and the secondary a normal main-sequence star, this would naturally explain our lack of detection as the brightness contrast would be very unfavourable, particularly if the secondary were to be rotating rapidly. This explanation would seem to be supported by the arguments in Section 5.1.

We explored this scenario further by using stellar evolution models from the MESA series (Paxton et al. 2011, 2013, 2015), seeking to match all observational constraints from our orbital fit and our spectroscopic analysis with a single isochrone placing the primary star either on the giant branch or near the clump, and the secondary star on the main sequence. We restricted the parameter space to $2.1 < \log g < 3.3$ and 4585 K $< T_{\rm eff} <$ 5150 K (following from our spectroscopic CCF and SPC estimates and their 1σ uncertainties), as well as $R > 26.3$ R$_\odot$ (Section 5.1). Solar metallicity was assumed.

A satisfactory solution was found for a primary star at the bottom of the giant branch with approximate parameters $M = 4$ M$_\odot$, $R = 26.6$ R$_\odot$, $\log g = 2.19$, $T_{\rm eff} = 4727$ K, $L = 313$ L$_\odot$, and an age of $\log(\text{age}) = 8.25$. These properties and the best-fitting isochrone are shown in Figure 7.

The mass of the secondary star for a given orbital inclination angle may be found from the primary mass and the spectroscopic mass function. We mark in Figure 7 three such values corresponding to representative inclination angles of 50, 70, and 90 degrees, which give secondary masses of 2.30, 1.77, and 1.63 M$_\odot$, respectively[8]. Other properties of the secondary inferred from the best-fitting isochrone are listed in Table 5. These results would suggest that the secondary star is no later than spectral type late A, and may be earlier

[8] Note that an inclination angle of 90° is actually ruled out by the lack of eclipses (see previous section).

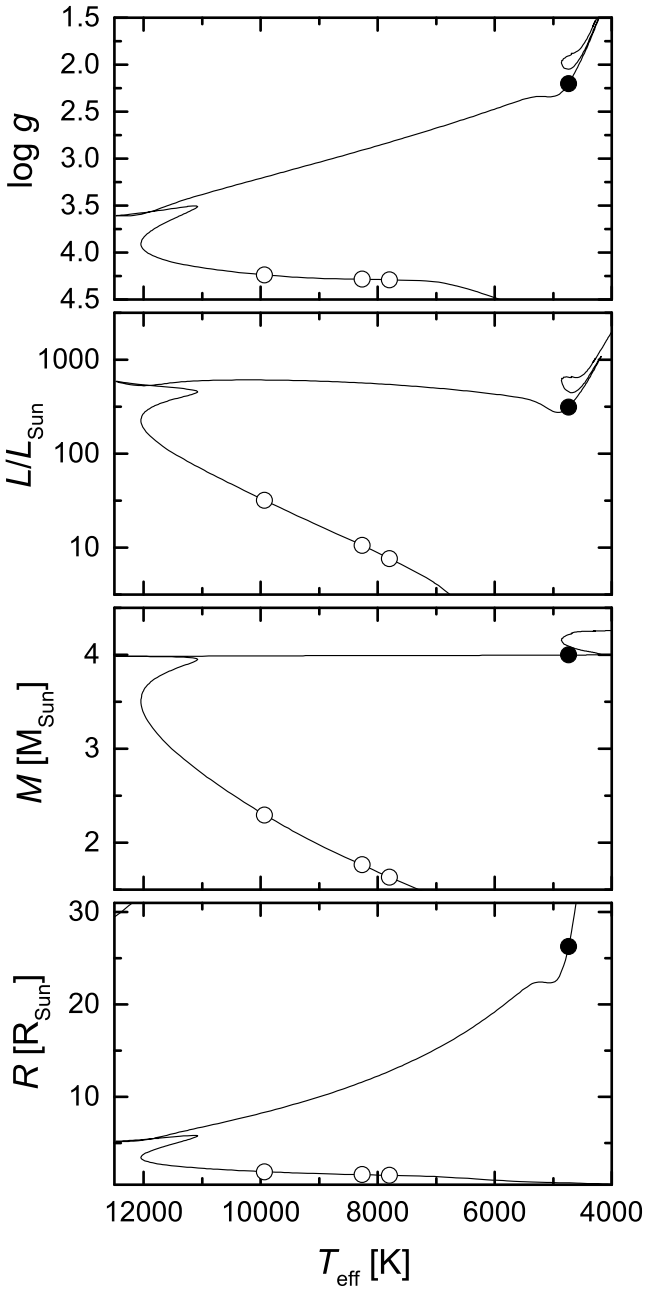

Figure 7. MESA model isochrone for an age of 178 Myr and solar metallicity. The filled circle near the top represents the primary component ($M_1 = 4$ M$_\odot$), and the open circles correspond to three possible secondary masses (2.30, 1.77, and 1.63 M$_\odot$) for representative inclination angles of 50, 70 and 90 degrees, respectively.

if lower inclination angles are assumed. The predicted luminosity ratios L_2/L_1 in Table 5 are seen to be fairly low, and this, compounded with the likely rapid rotation expected for an A-type star, would explain the non-detection of the secondary in our spectra.

An important information on the nature of V501 Aur is provided by the observed X-ray flux and resulting X-ray luminosity. Using the RASS count rate, $2.8(9)\times10^{-2}$ ct s^{-1}, the X-ray luminosity for the 1-σ range of the *Gaia* distance is from 8.7×10^{31} erg s^{-1} to 3.2×10^{32} erg s^{-1}. This is three

Table 5. Estimated absolute parameters of the secondary component for three representative inclination angles $i = 50$, 70 and 90 degrees. The table lists both bolometric and visual light ratios.

i [deg]	50	70	90
M [M$_\odot$]	2.30	1.77	1.63
L [L$_\odot$]	32	13	7.6
R [R$_\odot$]	1.9	1.60	1.5
$T_{\rm eff}$ [K]	9950	8260	7800
L_2/L_1 (bol)	0.10	0.041	0.024
L_2/L_1 (V)	0.11	0.055	0.033

orders more than a typical X-ray luminosity of late-type red giants, 10^{28} - 10^{29} erg s^{-1} (Maggio et al. 1990). The identification of the X-ray source with V501 Aur is, however, questionable. The position offset of the X-ray source is 19 arcsec and the RASS beam size about 30 arcsec. Hence, observations with better resolution are needed prior to any interpretation.

6 DISCUSSION AND FINAL REMARKS

Our new photometric and spectroscopic observations of V501 Aur have enabled us to revisit its properties in the context of previous claims that it is a WTTS belonging to the Taurus-Auriga star-forming region. Our spectroscopic observations reveal it to be a slightly eccentric, single-lined spectroscopic binary with an orbital period of about 68.8 days and a fairly massive unseen companion. No signs of eclipses are observed.

We have carried out a detailed investigation of the long-term photometric variability of V501 Aur using our own new data augmented with observations from several other sources, giving a total time span of two decades. The changes in the previously known photometric wave (in both period and amplitude), which has an average period of ∼55 days distinctly shorter than the orbital period, and the concomitant colour variations we have measured, suggest that the variability is caused by photospheric spots appearing at different stellar latitudes on a differentially rotating star. The long period of the photometric wave and the fairly rapid rotation of the visible component (~ 25 km s^{-1}) imply a large radius for the star of $R > 26.3$ R$_\odot$.

Such a large size is supported by our spectroscopic estimates of the surface gravity giving low values of $\log g = 2.3$–3.0. This strongly suggests it is an evolved star that must be far behind the Taurus-Auriga SFR. The systemic radial velocity of V501 Aur, -12.70 ± 0.08 km s^{-1}, is also inconsistent with the mean radial velocity of known members of Taurus-Auriga. Furthermore, our new measurements of the Li I λ6707 line show it to be much weaker than is typical for a young T-Tauri star, and the Hα line is not seen in emission, as would be expected. The distance of about 800 pc now known from the trigonometric parallax appearing in the first *Gaia* data release conclusively rules out a membership in the SFR. An independent distance estimate based on the minimum size of the star ($R \sin i$), its temperature, the apparent brightness, and a measure of interstellar extinction are perfectly consistent with the direct measurement. Thus,

the previous classification of V501 Aur as a WTTS belonging to Taurus-Auriga is overwhelmingly *not* supported by available observations.

Instead, the scenario that emerges for V501 Aur, aided by a comparison with stellar evolution models that succeed in matching all observational constraints, is one in which it is a background, non-eclipsing spectroscopic binary projected onto the Taurus-Auriga SFR, with a luminous, spotted, and fairly rapidly rotating giant star as the primary, and a likely much more rapidly rotating early-type star as the secondary. The estimated age of the system is roughly 180 Myr, according to the models. The unfavourable luminosity ratio of such a configuration along with the rotationally broadened lines expected for the secondary are sufficient to explain the non-detection of that star in our spectra. Another possible scenario is that the secondary component is a close binary.

V501 Aur may be related to a group of rapidly rotating giant stars recently identified in the photometry from the *Kepler* mission (Costa et al. 2015). Among them, we note that KIC 10293335 has properties somewhat similar to those of V501 Aur: $P_{\rm rot} = 55.96$ days (from a Fourier analysis), $T_{\rm eff} = 4363$ K, $\log g = 2.45$, $R = 21.29$ $R_\odot$, and $v \sin i = 12.7$ km s^{-1}. Interestingly, there are hints that this star may also be a (single-lined) spectroscopic binary. Further study of V501 Aur in the framework of a possible connection to this interesting class of stars would benefit from a detailed chemical analysis, including sensitive diagnostics of evolution such as the CNO abundances and the ^{12}C/^{13}C isotope ratio to help pinpoint its evolutionary state.

ACKNOWLEDGMENTS

We are grateful to A. Berndt, M. Moualla, T. Eisenbeiß, M. Hohle and T. Röll for help in obtaining the observations of V501 Aur at the University Observatory Jena. This work has been supported by the projects VEGA 2/0143/14, APVV-15-0458 and partially supported by SAIA scholarship. GT acknowledges partial support for this work from NSF grant AST-1509375. MV and TP would like to thank the European Union in the Framework Programme FP6 Marie Curie Transfer of Knowledge project MTKD-CT-2006-042514 for support. We would like to acknowledge financial support from the Thuringian government (B 515-070 10) for the STK CCD camera used in this project at the University Observatory Jena. The work of SS has been supported in part by the RFBR grant No. 15-02-06178 and NSh-9670.2016.2. SR acknowledges support from the People Programme (Marie Curie Actions) of the European Union's Seventh Framework Programme (FP7/2007-2013) under REA grant agreement No. [609305]. This paper has made use of data from DR1 of the WASP data as provided by the WASP consortium, and the computing and storage facilities at the CERIT Scientific Cloud, reg. no. CZ.1.05/3.2.00/08.0144 which is operated by Masaryk University, Czech Republic. This work has also made use of data from the European Space Agency (ESA) mission *Gaia* (http://www.cosmos.esa.int/gaia), processed by the *Gaia* Data Processing and Analysis Consortium (DPAC, http://www.cosmos.esa.int/web/gaia/dpac/consortium).
Funding for the DPAC has been provided by national institutions, in particular the institutions participating in the *Gaia* Multilateral Agreement. This article was created by the realisation of the project ITMS No.26220120029, based on the supporting operational Research and development program financed from the European Regional Development Fund.

REFERENCES

Blanco-Cuaresma, S., Soubiran, C., Jofré, P., Heiter, U. 2013, arXiv 1312.4545
Bouvier J., Wichmann R., Grankin K., et al. 1997, A&A, 318, 495
Buchhave, L. A., Latham, D. W., Johansen, A., et al. 2012, Nature, 486, 375
Buchhave, L. A., Bizzarro, M., Latham, D. W., et al. 2014, Nature, 509, 593
Butters O.W., West R.G., Anderson D.R., et al. 2010, A&A, 520, 10
Cardelli, J.A., Clayton, G.C., Mathis, J.S. 1989, ApJ, 345, 245
Carkner L., Mamajek E., Feigelson, E., et al. 1997, ApJ, 490, 735
Costa, A.D., Canto Martins, B.L., Bravo, J. P. et al. 2015, ApJ, 807, L21
Cox A.N. 2001, Allen's Astrophysical Quantities 4$^{\rm th}$ ed., Springer.
Daemgen S., Bonavina M., Jayawardhana R. et al. 2015, ApJ, 799, 155
D'Antona F., Mazzitelli I. 1994, ApJS, 90, 467
Drake, N.A.,2 Ramiro de la Reza,1 Licio da Silva,1 and David L. Lambert3
Ducati, J. R., Bevilacqua, C. M., Rembold, S. B., & Ribeiro, D. 2001, ApJ, 558, 309
European Space Agency 1997, The Hipparcos and Tycho Catalogues (ESA SP-1200), Noordwijk
Ferraz-Mello S. 1981, AJ, 86, 619
Flower, P. J. 1996, ApJ, 469, 355
Foster G. 1996, AJ, 112, 1709
Frink S., Röser S., Neuhäuser R., Sterzik M.F. 1997, A&A, 325, 613
Fűrész G. 2008, PhD thesis, Univ. Szeged
Gaia Collaboration, Brown A.G.A., Vallenari A., Prusti T., et al. 2016, A&A, special Gaia volume
Grankin K.N., Bouvier J., Herbst W., Melnikov S.Yu. 2008, A&A, 479, 827
Grankin K.N. 2013, AstL, 39, 251
Gray, D. F. 1992, The Observation and Analysis of Stellar Photospheres, Camb. Astrophys. Ser., Vol. 20, p. 430
Green, G.M., Schlafly, E.F., Finkbeiner, D.P. et al. 2015, ApJ, 810, 25
Henden, A., & Munari, U. 2014, Contributions of the Astronomical Observatory Skalnate Pleso, 43, 518
Høg E., Fabricius C., Makarov V.V., et al. 2000, A&A, 355, 27
Holdsworth D.L., Smalley B., Gillon M., et al. 2014, MNRAS, 439, 2078
Kholopov P.N., Samus N.N., Frolov M.S. et al., 1985, General Catalogue of Variable Stars, 4th Edition, Nauka, Moscow
Kharchenko, N. V., Piskunov, A. E., Röser, S., et al. 2009, A&A, 504, 681

Kurtz, M.J., Mink, D.J., Wyatt, W.F. et al. 1992, in Astronomical Data Analysis Software and Systems I, ASP Conf. Ser., Vol. 25, eds. D.M. Worral, C. Biemesderfer, and J. Barnes, 432
Latham, D.W. 1992, in IAU Coll. 135, Complementary Approaches to Double and Multiple Star Research, ASP Conf. Ser. 32, ed. H. A. McAlister & W. I. Hartkopf (San Francisco, CA: ASP), 110
Latham, D.W., Stefanik, R.P., Torres, G. et al. 2002, AJ, 124, 1144
Maggio, A., Vaiana, G.S., Haisch, B.M., Stern, R.A., Bookbinder, J., Harnden, F.R., Rosner, R. 1990, ApJ, 348, 253
Martín E.L., Magazzú A. 1999, A&A, 342, 173
Mooley, K., Hillenbrand, L., Rebull, L., Padgett, D., Knapp, G. 2013, ApJ, 771, 110
Mugrauer M. 2009, AN, 330, 419
Mugrauer M., Berthold T. 2010, AN, 331, 449
Munari, U., Zwitter, U. 1997, A&A, 318, 269
Nguyen D.C., Jayawardhana R., van Kerkwijk M.H., et al. 2009, ApJ, 695, 1648
Nordström B., Latham D.W., Morse, J. et al. 1994, A&A, 287, 338
Parimucha Š, Vaňko M. 2015, Living Together: Planets, Host Stars and Binaries, eds. by Slavek M. Rucinski, Guillermo Torres, and Miloslav Zejda. ASP Conference Series, 496, 309
Paxton, B., Bildsten, L., Dotter, A., et al. 2011, ApJS, 192, 3
Paxton, B., Cantiello, M., Arras, P., et al. 2013, ApJS, 208, 4
Paxton, B., Marchant, P., Schwab, J., et al. 2015, ApJS, 220, 15
Pollacco D.L., Skillen I., Collier Cameron A., et al. 2006, PASP, 118, 1407
Poznanski D., Prochaska J.X., Bloom, J.S. 2012, MNRAS, 426, 1465
Pribulla T., Garai Z., Hambálek Ľ., et al. 2015, AN, 336, 682
Randich, S., Gratton, R., Pallavicini, R., Pasquini, L., Carretta, E. 1999, A&A, 348, 487
Rucinski, S.M. 1992, AJ, 104, 1968
Smalley B., Kurtz D.W., Smith A.M.S., et al. 2011, A&A, 535, A3
Torres, G. 2010, AJ, 140, 1158
Vaňko M., Torres G., Pribulla T., et al. 2015, Living Together: Planets, Host Stars and Binaries, eds. by Slavek M. Rucinski, Guillermo Torres, and Miloslav Zejda. ASP Conference Series, 496, 262
Wichmann R., Krautter J., Schmitt J.H.M.M., et al. 1996, A&A, 312, 439
Wichmann R., Torres G., Melo C.H.F., et al. 2000, A&A, 359, 181
Woźniak P.R., Vestrand W.T., Akerlof C.W., et al. 2004, AJ, 127, 2436
Zucker, S., & Mazeh, T. 1994, ApJ, 420, 806